Crossover from ferromagnetic superconductor to superconducting ferromagnet in P-doped $EuFe_2(As_{1-x}P_x)_2$

S. Yu. Grebenchuk,[1,2] Zh. A. Devizorova,[1] I. A. Golovchanskiy,[1,3,4] I. V. Shchetinin,[4] G.-H. Cao,[5] A. I. Buzdin,[6,7] D. Roditchev,[8,1] and V. S. Stolyarov[1,3,*]

[1]*TQPSS Laboratory, Moscow Institute of Physics and Technology, 141700 Dolgoprudny, Russia*
[2]*Skolkovo Institute of Science and Technology, 121205 Moscow, Russia*
[3]*SQT Laboratory, Dukhov Research Institute of Automatics (VNIIA), 127055 Moscow, Russia*
[4]*National University of Science and Technology MISIS, 119049 Moscow, Russia*
[5]*Department of Physics, Zhejiang University, Hangzhou 310027, China*
[6]*University Bordeaux, LOMA, F-33405 Talence, France*
[7]*Sechenov First Moscow State Medical University, Moscow 119991, Russia*
[8]*Laboratoire de Physique et d'Etudes des Materiaux, LPEM, UMR-8213, ESPCI-Paris, PSL, CNRS, Sorbonne University, 75005 Paris, France*

(Received 26 April 2020; revised 12 September 2020; accepted 14 September 2020; published 1 October 2020)

In P-doped pnictide, $EuFe_2(As_{1-x}P_x)_2$ superconductivity coexists with a ferromagnetism of Eu-4f spins. Above $x \simeq 0.26$, superconductivity vanishes whereas ferromagnetism remains. Here, we focus on the crossover region and study two $EuFe_2(As_{1-x}P_x)_2$ single crystals with $x = 0.21$ and $x = 0.25$; the superconducting critical temperature of the first one is slightly higher and of the second one is slightly lower than the Curie temperature. Despite similar compositions, characteristic temperatures and bulk magnetic properties of the two systems, their local magnetic structures and superconducting vortex-antivortex phases are found drastically different. We demonstrate that the interplay between superconductivity and magnetism is strongly dominated by the superconducting order in the first system, whereas it is mainly governed by ferromagnetism in the second one. Our discovery raises several fundamental questions on the vortex nucleation and dynamics in magnetic superconductors.

DOI: 10.1103/PhysRevB.102.144501

I. INTRODUCTION

The coexistence of ferromagnetism (FM) and singlet superconductivity is a very rare phenomenon. Usually, the exchange energy is large compared to the superconducting condensation energy, and the exchange field is strong enough to align the electron spins, thus, destroying the spin-singlet structure of Cooper pairs via the so-called paramagnetic effect [1]. Recently, the coexistence of the two orders has been reported in P-doped $EuFe_2As_2$ pnictide [2–10], Fig. 1(a). Surprisingly high superconducting critical temperatures up to $T_{SC} \approx 25$ K, where (SC) represents supercurrent, were observed, close to the Curie temperatures $T_{FM} = 15$–25 K. This provides the unique opportunity for studying the interplay between the two orders. Although, the triplet superconductivity could coexist with strong ferromagnetism. Such a situation is expected in superconducting ferromagnets UGe_2, URhGe, and UCoGe [11]. In these compounds, the Curie temperature T_{FM} is substantially higher than T_{SC}, and superconductivity appears when a strong ferromagnetic order already exists. As a result, the superconductivity exists only in a domain-driven vortex (V) state [12], the Meissner phase is absent.

Several experimental and theoretical studies concluded that the superconducting condensate in $EuFe_2(As_{1-x}P_x)_2$ involves singlet Cooper pairs [13–15]. In general, the Fe-3d electrons dominate the transport properties, whereas Eu-4f states lay deeply below the Fermi level and are responsible for magnetism. As the exchange field is low, it only weakly affects the spins of the Cooper pairs. The main interaction between the two orders is, therefore, electromagnetic one [15]. Since the two orders have essentially different magnetic structures, their interplay could lead to nontrivial phase diagram and peculiar magnetic patterns [8,15]. Note that the present case is drastically different from the one previously observed in reentrant ferromagnetic superconductors $ErRh_4B_4$ [16] and $HoMo_6S_8$ [17] where the exchange interaction dominates over the electromagnetic one (for details, see Ref. [1]). The weakness of the exchange interaction in $EuFe_2(As_{1-x}P_x)_2$ enables superconductivity and ferromagnetism to coexist in an unusually broad range of compositions and temperatures. Moreover, on the phase diagram, Fig. 1(b), the superconducting dome intercepts the ferromagnetic phase at P-content $x \simeq 0.24$. This gives an unprecedented opportunity to study the crossover between "ferromagnetic superconductivity" with $T_{SC} > T_{FM}$ and "superconducting ferromagnetism" $T_{SC} < T_{FM}$.

In this paper, we focus on the crossover region $T_{SC} \approx T_{FM}$ of the phase diagram of the ferromagnetic superconductor $EuFe_2(As_{1-x}P_x)_2$. We provide global (magnetization, transport) and local (MFM) studies on two single crystals with

*Correspondence requests for materials should be addressed to V. S. Stolyarov; vasiliy.stoliarov@gmail.com.

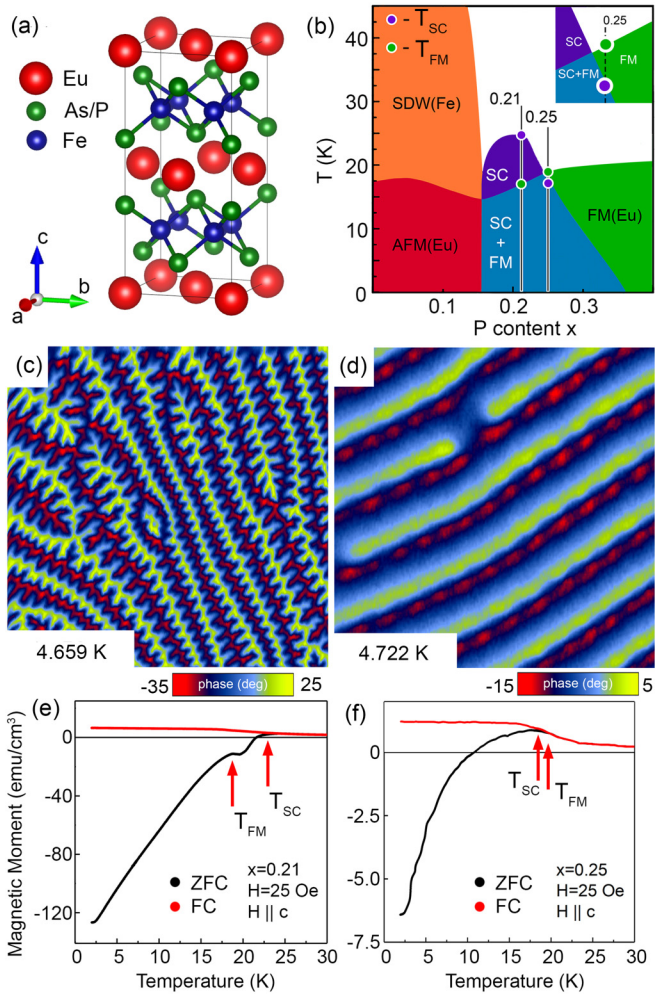

FIG. 1. (a) Schematics of $EuFe_2(As_{1-x}P_x)_2$ crystal lattice; (b) phase diagram of $EuFe_2(As_{1-x}P_x)_2$ as a function of x [19]. Vertical lines correspond to P contents studied in this paper. Green and indigo circles denote, respectively, the Curie temperature T_{FM} and the superconducting critical temperature T_{SC} of the two samples. (c) and (d) $6 \times 6\ \mu m^2$ magnetic force microscopy (MFM) maps measured at low temperatures in the $x = 0.21$ sample (c), and in the $x = 0.25$ sample (d). (e) and (f) Temperature dependencies of the zero-field-cooled (ZFC) and field-cooled (FC) magnetization $M(T)$ of $x = 0.21$ sample (e) and of the $x = 0.25$ sample (f). The magnetic field was applied along the c axis, that is, perpendicular to the surface studied by MFM in (c) and (d).

$x = 0.21$ ($T_{SC} \approx 22$ K $> T_{FM} \approx 18$ K) and $x = 0.25$ ($T_{SC} \approx 18.4$ K $< T_{FM} \approx 19.3$ K). Despite almost identical T_{FM} of the two samples, we find substantial differences in their magnetic domain structures [see Figs. 1(c) and 1(d)], global magnetization [see Figs. 1(e) and 1(f)], and the temperature evolution of the domains (see Fig. 2). We suggest that, in the sample with $x = 0.25$, the ferromagnetic order decides the magnetic structure. On the contrary, in the crystal with $x = 0.21$, it is the superconducting order that dominates at the onset of ferromagnetism at $T_{FM} < T_{SC}$, resulting in unusually narrow magnetic domains and, at lower temperatures, in a spontaneous generation of superconducting vortex-antivortex (V-A) pairs. Moreover, deep below T_{FM}, the vortex-antivortex distribution in the domain vortex phase [8,18] is found to be significantly different in the ferromagnetic superconductor $x = 0.21$ as compared to superconducting ferromagnet $x = 0.25$ (Fig. 2). We argue that considering a partial reconnection of the magnetic flux inside the samples could explain the differences observed in MFM maps.

II. RESULT

The crystal structure of $EuFe_2(As_{1-x}P_x)_2$ is presented in Fig. 1(a). Phosphorus substitutes As atoms in the parent $EuFe_2As_2$ compound and creates a "chemical pressure" that modifies the interlayer distance, thus, influencing the material's properties. Depending on P-content x, the phase diagram of $EuFe_2(As_{1-x}P_x)_2$, presented in Fig. 1(b), contains different magnetic phases [19]. The most intriguing region is in the vicinity of $x = 0.20$ where the superconducting dome coexists with ferromagnetism. Generally, the superconducting critical temperature T_{SC} is higher than the Curie temperature T_{FM}; it rapidly vanishes for $x > 0.26$. We found a region around $x = 0.25$ where the superconducting critical temperature is still high enough to enable experimental studies, but it is already lower than the Curie temperature $T_{SC} \lesssim T_{FM}$.

The magnetization of $EuFe_2(As_{1-x}P_x)_2$ crystals was measured using a vibrational magnetometer. MFM experiments were provided in the temperature range of 4–30 K using CoCr-covered silicon cantilevers. The samples were cleaved prior to their studies (further experimental details and additional results of the sample characterization are available in Appendices A, D, and E).

The global magnetization curves $M(H)$ confirmed the expected out-of-plane easy magnetization axis at $T < T_{FM}$. The ferromagnetic properties of the both samples are very close: at 5 K, the saturation magnetization in the $x = 0.21$ sample was 1.29 T (1.32 T in the $x = 0.25$ sample), anisotropy field 0.44 (0.48) T. These values provide the domain wall width $\simeq 11$ nm and the exchange stiffness constant $\simeq 0.33 \times 10^{-11}$ J/m for the $x = 0.25$ sample (details of the calculations are presented in Appendix A) as expected for a ferromagnet with such a low Curie temperature. In contrast, in the $x = 0.21$ sample, the domain-wall width $\simeq 6$ nm and the exchange stiffness constant $\simeq 0.09 \times 10^{-11}$ J/m were found, that is well below typical values. If this sample had a "normal" exchange stiffness of the $x = 0.25$ one, its domain width would be $\simeq 0.48\ \mu$m, that is larger than the observed values of 0.15–0.35 μm, Fig. 1(c). This discrepancy witnesses for a strong influence of the superconductivity on ferromagnetism in the $x = 0.21$ sample, resulting in a shrink of ferromagnetic domains [20].

Temperature dependencies of magnetization $M(T)$ of ZFC and FC samples are shown in Figs. 1(e) and 1(f). FC $M(T)$ curves of both samples are similar: a constant positive (ferromagnetic) signal at low temperatures, followed by a progressive decrease to zero above $\approx$18–19 K. This is consistent with the expected transition at T_{FM} from a ferromagnetic state to a paramagnetic one due to an Eu^{2+} sublattice [7,19,21]. Note, that a tiny amount of ferromagnetic impurities Fe_2P with $T_{FM} \sim 306$ K was previously detected in similar crystals [19]; it could also be responsible for the revealed paramagnetic trend. The recorded ZFC $M(T)$ curves

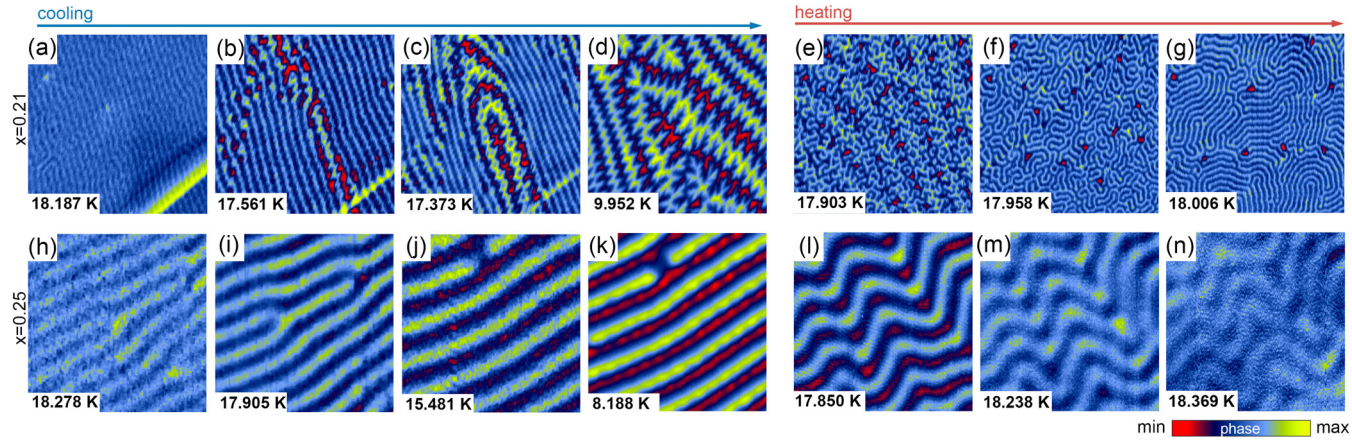

FIG. 2. MFM maps of the out-of-plane magnetization component measured in $EuFe_2(As_{1-x}P_x)_2$ samples with P-contents $x = 0.21$ [upper row (a)–(g)], and $x = 0.25$ [lower row (h)–(n)] upon cooling (blue arrow) and heating (red arrow); full dataset is available in the Supplemental Material [22]. The scan area ($6 \times 6\ \mu m^2$) and color code are the same as in Figs. 1(c) and 6(d).

are different. In the $x = 0.21$ sample, a clear diamagnetism is observed below $\approx$22 K, consistent with the measured resistive transition to the superconducting state. The transition to the ferromagnetic state at 18 K produces only a kink, not a significant change in the overall trend. The diamagnetic ZFC $M(T)$ dominates at low temperatures: At 2 K, it is by a factor of $\sim$20 higher than the FC $M(T)$ signal. In the $x = 0.25$ sample, the diamagnetic ZFC $M(T)$ signal is only by a factor of $\sim$5 higher than the FC one. Moreover, upon increasing temperature, the diamagnetism of the $x = 0.25$ sample rapidly vanishes. Already above 11 K, the ZFC $M(T)$ signal is dominated by ferromagnetism, whereas the sample is still superconducting. Thus, compared to the $x = 0.21$ case, the diamagnetism in the $x = 0.25$ sample is significantly (by a factor of $\sim$4) weaker, suggesting a stronger influence of ferromagnetism on superconductivity in this sample.

III. DISCUSSION

Strong differences in the magnetic behavior of the two close systems are further revealed in MFM maps (full set is presented in the Supplemental Material [22] in Secs. A and B, SFigs. 1–3). In the $x = 0.21$ sample, the ferromagnetism sets in at $T_{FM} = 18$ K when the superconductivity is already well established. As a result, the emerging magnetic domains are very narrow [see Fig. 2(a)], i.e., on the order of the London penetration depth $\lambda = 150$–400 nm in this superconductor. It is much smaller than what the FM subsystem would manifest in the absence of superconductivity [23]. The underlying physics, here, is related to the energy of Meissner currents that tend to screen the magnetization of emerging magnetic domains. Having large magnetic domain structures would result in a much higher-energy cost. Since the ferromagnetism at $T \lesssim T_{FM}$ is very weak as compared to the superconducting order, the thermodynamic equilibrium is reached by reducing the magnetic domain width. With a decrease in the temperature, however, the increasing magnetization provokes a spontaneous generation of vortex-antivortex pairs [see Fig. 2(b)]. Vortices and antivortices fill the respective up- and down-oriented magnetic domains [see Fig. 2(c)], relax the screening supercurrents and reduce the corresponding energy cost. As a result, at low temperatures, the domain width is increased [see Fig. 2(d)] [8]. Note that, at low temperatures, the density of vortices and antivortices is so high that they are not resolved individually in MFM maps anymore.

The MFM maps acquired in the $x = 0.25$ sample are presented in Figs. 2(h)–(k). At $T = 18.278$ K, the sample is just below the superconducting transition but already 1 K below T_{FM}. Due to strong magnetization of the domains ($\sim$0.4 T, see Appendix A), superconductivity nucleates directly in a dense vortex-antivortex state. Although, the superconducting suborder is weak as compared to the FM one, and the sample globally behaves, such as an ordinary FM film, manifesting a typical striped domain structure slowly evolving with temperature [see Figs. 2(h)–(k)]. The size of these domains is significantly larger than in Fig. 2(a); yet it is basically the same as in Fig. 2(d). Note that close widths of relaxed FM domains of the two samples are, indeed, expected as they have close thicknesses (12 and 14 μm), compositions and T_{FM}. The observed behavior indicates that domain structures in the $x = 0.25$ sample are controlled essentially by the ferromagnetic subsystem. From this perspective, it is similar to the artificial Nb/Py superconductor-ferromagnet hybrids [24,25].

At low temperatures, dense vortex and antivortex lattices in the $x = 0.25$ sample become spatially inhomogeneous, Figs. 2(j) and 2(k). The density of the vortex (antivortex) lattice is modulated along the domain walls; the maxima (antimaxima) of modulations are "in phase." Moreover, they approach and form "dimers" across the domain walls (further details can be found in Appendix E). The modulation effects result from a competition between attractive and repulsive terms in the interaction potential which still need to be determined.

Further differences are revealed upon thermal cycling (follow Fig. 2 row by row from left to right). Upon cooling the $x = 0.21$ sample below T_{FM}, straight narrow domains appear [see Fig. 2(a)] constrained by Meissner screening currents. At low temperatures, these narrow domains are transformed into large branched domains filled with vortices and antivortices, Fig. 2(d). When the sample is warmed up again, the branched domain structure transforms back into the narrow domain one [see Figs. 2(e)–(g)]. The width of these narrow domains is

quite the same as that observed upon cooling [Fig. 2(a)]. The domains are not straight, however, but form a maze. The transition from large branched domains to narrow maze structure occurs in the vicinity of T_{FM} where the ferromagnetic suborder is much weaker than the superconducting one. In this temperature window, most of vortex-antivortex pairs have already annihilated, and only strongly pinned vortices and antivortices remain, visible in Figs. 2(f) and 2(g) as randomly dispersed bright and dark spots. These vortices pin narrow (vortex-free) domains and decide the maze pattern. As the temperature is further increased, vortex and antivortex progressively depin and annihilate, leading to more and more regular maze patterns. Thus, near T_{FM}, the magnetic network in the $x = 0.21$ sample is controlled by the superconducting suborder. If the sample is warmed above T_{FM} to a temperature at which no vortex remains and then cooled down again, the straight domain structure of Fig. 2(a) reappears.

In the $x = 0.25$ sample, large domains are preserved over the entire temperature window $T < T_{FM}$ (follow the corresponding row in Fig. 2), witnessing for the dominant role of ferromagnetism. Although upon warming, when the temperature approaches T_{SC}, the domains start to twist [compare Figs. 2(k) and 2(l)]. As in the case of the $x = 0.21$ sample, vortices and antivortices generated upon cooling start to annihilate. As the density of vortices decreases, the remaining vortices and antivortices can move more freely along their respective domains. The mutual attraction between vortices and antivortices and the repulsion between the vortices of the same polarity lead to vortex-antivortex clustering and, in some locations, to a quasiregular networks [see Fig. 2(l)]. There, vortex-antivortex chains are formed. The relative phase between the chains maximizes the distance between vortices of the same polarity, thus, reducing the vortex interaction energy.

Spectacular spatial patterns in Fig. 2 raise several fundamental questions. The first one is the microscopic mechanism of the simultaneous generation of vortex-antivortex pairs. In nonmagnetic superconductors, quantum vortices own line-shaped 2π-phase singularities around which vortex current loops form (see Appendix C). These vortices always nucleate individually at the edges of the specimen. How do the vortex-antivortex pairs nucleate inside the ferromagnetic $EuFe_2(As_{1-x}P_x)_2$? Do they appear as close pairs of line-shaped $+2\pi$ and -2π phase singularities crossing all the sample, or they first nucleate as tiny singular loops (see Fig. 9) in Appendix C that further grow up along the walls to finally emerge as vortex-antivortex pairs at surface? Are the nucleation processes the same in both studied systems? The second question is related to the peculiar field distribution inside ferromagnetic superconductors. Experimentally, we observed a difference, by a factor of 3, in the contrast between MFM maps from $x = 0.21$ and $fx = 0.25$ samples [see the color scale bars in Figs. 1(c) and 1(d)], despite similar magnetization ∼1.3 T of domains in both samples. This difference could be partially attributed to experimental conditions (slightly different tip sensitivities, for instance), although it might also be related to the different magnetic-field distribution in the samples due to interaction of ferromagnetism with superconductivity. It is useful to recall the magnetic-field distribution in thin nonsuperconducting ferromagnetic films with a perpendicular magnetization (see Fig. 3). There, some

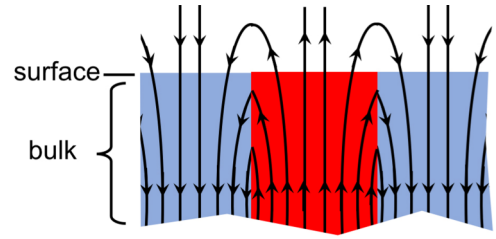

FIG. 3. Schematic of the magnetic field inside and outside a thin ferromagnet with the magnetization perpendicular to its surface. The red and blue regions represent up- and down-oriented FM domains; narrow domain walls are considered. A significant part of magnetic lines reconnects at the domain walls, forming closed loops.

magnetic lines reconnect inside the sample and form loops. The reconnections could be continuous [26,27] or via domains with in-plane magnetization [28,29]. These loops escape from observation by MFM which detects the magnetic lines getting out of the surface. Since superconducting vortices are expected to follow the magnetic lines, one can anticipate that vortices and antivortices situated on the opposite sides of the same domain wall may reconnect inside the sample to form vortex loops [30]. However, bending vortex lines in loops has an additional energy cost. Usually, the vortex bending radius in superconductors is limited by the London penetration depth λ. This limitation is more constraining for the $x = 0.21$ sample due to its short-scale domain branching, Figs. 1(c) and 2(d), leading to a lower number of reconnections and, thus, explaining a higher MFM contrast observed in this sample as compared to the $x = 0.25$ one. On the other hand, the magnetic line reconnections could be attenuated in both samples due to a high value of magnetization inside the domains ∼1.3 T. Because of such a strong field, the vortex (and antivortex) lattices in neighboring domains are very dense: the intervortex distance is ∼45 nm there, that is significantly shorter than λ. If, due to a mutual attraction between vortex and antivortex lattices, such a high vortex (antivortex) density is preserved near domain walls, the vortex loop formation might become problematic. The above-mentioned questions are complex problems that require further experimental studies and theoretical considerations beyond the Ginzburg-Landau limit of weak-order parameters.

IV. CONCLUSION

To sum up, in this paper, we focused on the crossover region of the phase diagram of the ferromagnetic superconductor $EuFe_2(As_{1-x}P_x)_2$ where, upon increasing P-content x, the superconducting critical temperature T_{SC} was expected to cross the Curie temperature T_{FM} of the ferromagnetic transition. We synthesized single crystals of this compound, studied their superconducting and magnetic properties, and showed that in the sample with $x = 0.21$ T_{SC} is still a bit higher than T_{FM}, whereas in the specimen with $x = 0.25$, it is already lower than T_{FM}. Our global (magnetization) and local (magnetic force microscopy mapping) experiments demonstrated that, despite close T_{SC} and T_{FM} in both samples, the magnetic properties of the sample with $T_{SC} \gtrsim T_{FM}$ are dominated by superconductivity whereas it is the ferromagnetic order that

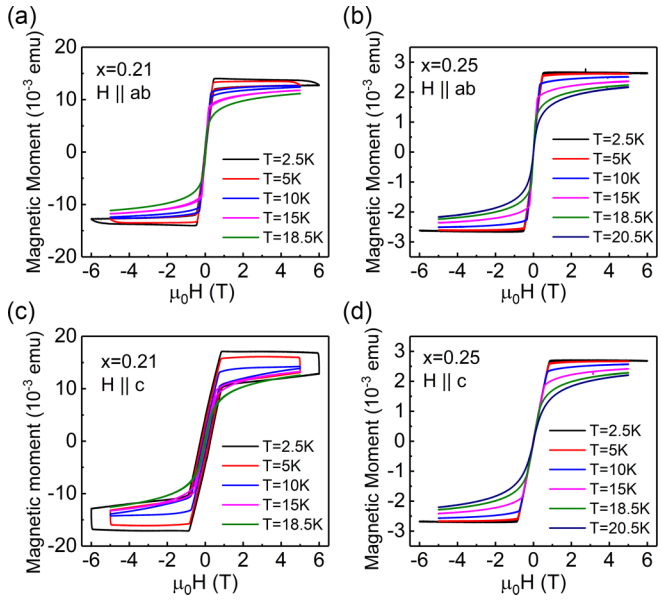

FIG. 4. $M(H)$ magnetization curves of the $x = 0.21$ and $x = 0.25$ samples measured with the magnetic field aligned along (a) and (b) and across the crystal c axis (c) and (d).

governs them in the crystal with $T_{SC} \lesssim T_{FM}$. This justifies a distinct identification of these similar materials as ferromagnetic superconductors and superconducting ferromagnets, respectively.

ACKNOWLEDGMENTS

We are grateful to L. Y. Vinnikov for fruitful discussions, to I. S. Veshchunov, N. Zhou, Z. Shi, and W. Jiao for providing the samples and to D. Baranov, R. Hovhannisyan, and A. Astrakhantseva for technical support. The authors acknowledge the Russian Science Foundation (Project No. 18-72-10118) for support in experiments and the Ministry of Science and Higher Education of the Russian Federation (Project No. 0718-2020-0025) for support in sample characterizations. Z.A.D. is grateful to the Foundation for the advancement of theoretical physics "BASIS." D.R. acknowledges French ANR grant SUPERSTRIPES. D.R. and A.I.B. acknowledge COST Action CA16218–Nanoscale Coherent Hybrid Devices for Superconducting Quantum Technologies. G.-H.C. acknowledges support from the National Key Research and Development Program of China (Grant No. 2016YFA0300202).

APPENDIX A: MAGNETIZATION MEASUREMENTS AND MAGNETIC DOMAIN STRUCTURE CALCULATIONS

The ferromagnetic domain structure was analyzed combining results of MFM imaging and magnetization measurements $M(H)$ using the Kittel model of striped domains in ferromagnetic thin films [31] as follows.

Figure 4 shows the $M(H)$ dependencies at various temperatures. One notes that $M(H)$ curves of the two samples are characterized by close saturation fields and are very similar in general. However, $M(H)$ measured with $H \parallel ab$ in the $x = 0.21$ sample, Fig. 4(a), shows an unusual vertical hysteresis

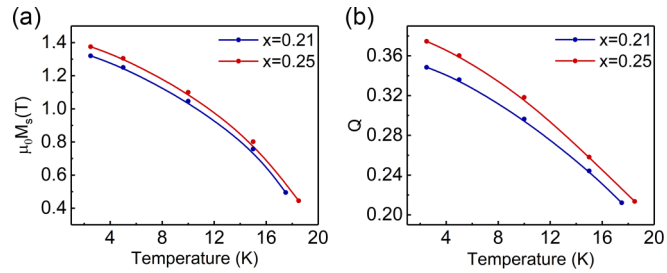

FIG. 5. (a) Temperature dependence of the saturation magnetization M_s and (b) of the quality factor Q.

at low temperatures [clearly visible on red and black $M(H)$ curves, acquired at 5 and 2.5 K, respectively], which is not observed in the $x = 0.25$ sample, Fig. 4(b). Moreover, a larger hysteresis is observed in $M(H)$ of the $x = 0.21$ sample when the field is applied $H \parallel c$ [compare Figs. 4(c) and 4(d)]. In superconductors, such a hysteresis is related to the Abrikosov vortex pinning. We, therefore, may suggest that, for some reasons, the vortex pinning in the $x = 0.21$ sample is significantly larger than in the $x = 0.25$ one. We come back to this point at the end of the Appendix.

Since the crystals are ∼1 mm large in the ab-crystallographic direction and only $d \sim 10$-μm thick in the c-oriented out-of-plane direction, the considered geometry is essentially that of thin films. At high magnetic fields, the diamagnetism due to superconductivity is suppressed, and the magnetization is dominated by ferromagnetism. In this case, the large saturation field $\mu_0 H_{s(ab)}$ of the magnetization measured with in-plane applied magnetic field (that is parallel to the ab axes) implies that the easy magnetization axis is the c axis and the easy orientation is the out-of-plane orientation. This statement is supported by the well-developed striped domain structure observed with MFM. Thus, the saturation field for the in-plane orientation of magnetic field is $H_{s(ab)} = H_a$, and for the out-of-plane orientation of magnetic-field $H_{s(c)} = M_s - H_a$, where $H_a = 2K_u/\mu_0 M_s$ is the out-of-plane anisotropy field, K_u is the out-of-plane anisotropy constant, and M_s is the saturation magnetization. Figure 5 shows the temperature dependence of the saturation magnetization $M_s(T)$ and of the quality parameter $Q(T) = H_a/M_s$; they are derived from magnetization curves in Fig. 4. According to Fig. 5, ferromagnetic properties of both samples are very close: at 5 K, the saturation magnetization in the $x = 0.21$ sample is $M_s = 1.29$ T (1.32 T in the $x = 0.25$ sample), the anisotropy field is $H_a = 0.44$ T (0.48 T in the $x = 0.25$ sample).

As a next step, the domain structure of samples is quantified. Figure 6 shows the temperature dependence of the domain width W. The latter was estimated directly from MFM images. Branching effects on the domain structure of the $x = 0.21$ sample were not taken into account.

According to the MFM studies, the following condition is fulfilled: $\delta \ll W \ll d$, where δ is the domain-wall width, and d is the thickness of studied samples. Therefore, the conventional Kittel model of the domain structure [31] can be applied,

$$\delta = \pi W^2/3.84^2 Qd, \tag{A1}$$

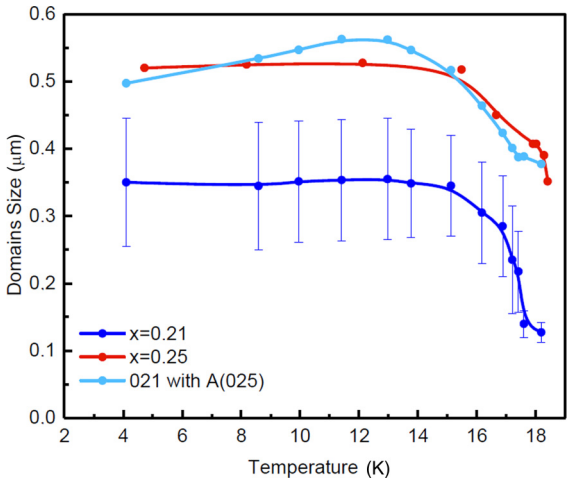

FIG. 6. Temperature dependence of the domain width $W(T)$. Despite similar magnetization and thickness, the domain width in the $x = 0.21$ sample (blue curve) is significantly smaller than in the $x = 0.25$ one (red curve). The cyan curve shows the hypothetical temperature dependence of the domain width in the $x = 0.21$ sample calculated using $A(T)$ of the $x = 0.25$ sample (see Fig. 7). The match with the experimental red curve witnesses for a much more important role played by superconductivity in the magnetism of the $x = 0.21$ sample as compared to the $x = 0.25$ one.

where $\delta = \pi\sqrt{A/K_u}$ and A is the exchange stiffness constant.

Figure 7 shows the temperature dependencies of the calculated domain-wall width $\delta(T)$ and the exchange stiffness constant $A(T)$. One sees that despite very close T_{FM}, d, $M_s(T)$, and $Q(T)$ of the two samples, the calculated microscopic parameters are essentially different. For instance, at 5 K, the domain-wall width $\delta \simeq 11$ nm and the exchange stiffness constant $A \simeq 0.3 \times 10^{-11}$ J/m for the $x = 0.25$ sample, which are rather expected values for a ferromagnet with a low Curie temperature. In contrast, the calculated magnetic parameters for the $x = 0.21$ sample, $\delta \simeq 6$ nm and $A \simeq 0.09 \times 10^{-11}$ J/m, are well below typical values and are radically different from the parameters of the $x = 0.25$ sample.

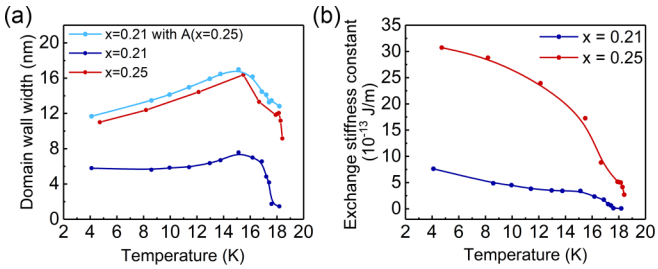

FIG. 7. (a) Calculated temperature dependence of the domain-wall width $\delta(T)$ and (b) corresponding exchange stiffness constant $A(T)$. The calculations are performed using the data presented in Figs. 5 and 6. The light blue curve shows the hypothetical $\delta(T)$ dependence in the $x = 0.21$ sample calculated using $A(T)$ of the $x = 0.25$ sample. The match with the red curve demonstrates almost identical magnetic properties of the two samples (in the absence of superconductivity).

The above discrepancies, and specifically, very different–by factors of 4–6—exchange stiffness constants of the two samples look strange, as one would expect the two systems to have close microscopic magnetic parameters. We can, thus, suppose that the superconducting order plays a significant role in the formation of magnetic patterns, in particular, in the $x = 0.21$ sample with its higher T_c. To start, let us consider that this sample has intrinsically the same exchange stiffness constant as the $x = 0.25$ crystal. Taking $A \simeq 0.3 \times 10^{-11}$ J/m for the $x = 0.21$ sample, we get new estimates for the hypothetical domain-wall width δ and the wall width W; the results are presented as cyan curves in Figs. 7 and 6, respectively. The remarkable match with the data extracted from the experiments on the $x = 0.25$ sample seems to confirm our hypothesis about a strong influence of superconducting suborder on magnetic structures of the $x = 0.21$ system and, by comparison, its much weaker effect on the $x = 0.25$ sample. In particular, this interplay might be on the origin of the ferromagnetic domain shrinking as suggested in Refs. [15,20], and possibly of the domain branching in the $x = 0.21$ sample. Note, however, that the domain branching is known to appear in nonsuperconducting ferromagnets as well and, thus, establishing the role of superconductivity in the formation of dendritic patterns observed in our paper requires further investigations. Regardless of the origin of dendrites, they clearly play the role of vortex pinning centers. Their presence could explain the vertical hysteresis observed in $M(H)$ curves of the $x = 0.21$ sample, Figs. 4(a) and 4(c), and its absence in the $x = 0.25$ one, Figs. 4(b) and 4(d).

APPENDIX B: VORTEX PHASE SINGULARITY

This section is devoted to the topology of the phase transition in ferromagnetic superconductors ($T_c > T_{FM}$, as in our $x = 0.21$ sample) from the domain Meissner state with no vortices inside to the domain vortex state. The MFM maps across this transition are presented in Figs. 2(a)–2(d) of the regular text.

In nonmagnetic type II superconductors, subject to the magnetic field, vortices nucleate individually at the sample edges (that are macroscopically far from the regions studied in this paper) and, then, move inside the sample. The reason is the quantization in superconductors of the so-called winding number. Precisely, any closed loop $\vec{l}$ inside a quantum condensate (a superconductor but also a cloud of Bose condensed cold atoms, or a superfluid, etc.) encloses an integer number of 2π phase singularities $\oint_{\text{loop}} \vec{\nabla}\phi\, d\vec{l} = 2\pi n$ with $n = 0, \pm 1, \pm 2, \ldots$, called the "winding number." This is a general consequence of the continuity and unievaluation of the quantum-mechanical wave-function $\psi = |\psi|e^{i\phi}$, where ϕ is the phase. For these reasons, one can always consider a closed loop along the sample edge and find the corresponding winding number n. Since n is quantized, the only possibility to modify it is to break the loop. This is exactly what the vortices do when they enter into quantum condensates from the edges. The core of each quantum vortex contains a single 2π-phase singularity—a line around which the phase of the condensate's wave function accumulates exactly one 2π shift, $\oint_{\text{vortex}} \vec{\nabla}\phi\, d\vec{l} = \pm 2\pi$ [see Fig. 8(a)]. Indeed, taking the

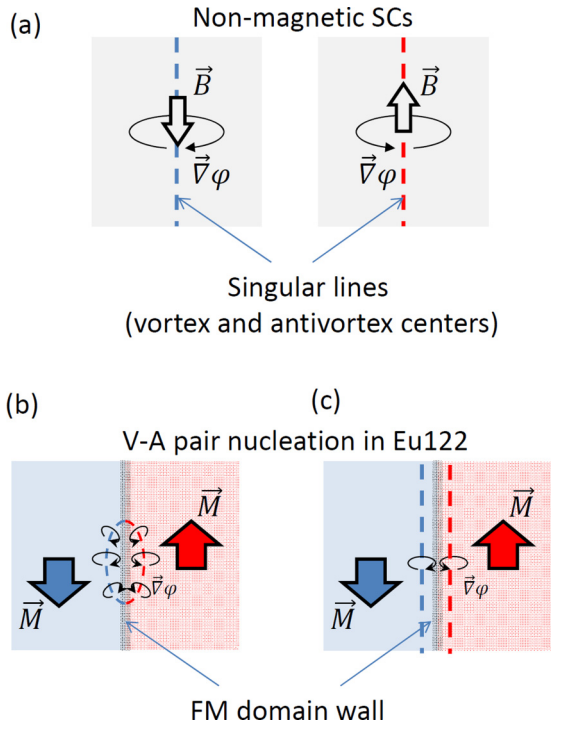

FIG. 8. Vortex and antivortex phase singularities (blue and red dashed lines) in nonmagnetic and ferromagnetic SCs. Loops with arrows depict the phase gradients.

integral over a loop of a radius r leads to the phase gradient along the loop to be $|\vec{\nabla}\phi| = 1/r$, which diverges at $r \to 0$ and justifies the term singularity or singular line. The phase gradient $\vec{\nabla}\phi$ is the reason why supercurrents (vortex currents) circulate around the singular line,

$$\vec{j}_{\text{vortex}} = -\frac{i\hbar e}{2m^*}(\psi^*\vec{\nabla}\psi - \psi\vec{\nabla}\psi^*) = \frac{\hbar 2e}{m^*}|\psi|^2\vec{\nabla}\phi. \quad \text{(B1)}$$

This expression can be presented in a simple form

$$\vec{j}_{\text{vortex}} = (2e)n_s\vec{v}_s, \quad \text{(B2)}$$

where $2e$ is the charge of the Cooper pairs, $n_s = |\psi|^2$—their concentration, and $\vec{v}_s = \frac{\hbar}{m^*}\vec{\nabla}\phi$ is the superfluid velocity. One immediately sees that $\vec{v}_s$ diverges towards the phase singularity position $|\vec{v}_s(\vec{r} \to 0)| = \frac{\hbar}{m^*|\vec{r}|}(\vec{r} \to 0) \to \infty$. At the same time, the amplitude of the order parameter and the vortex currents vanish, $|\psi(\vec{r} \to 0)| \to 0$, thus, keeping the kinetic energy finite. This is why, in any quantum condensate, the order parameter in the center of the vortex core is completely suppressed. Note that the magnetic flux due to vortex currents exists only owing to the electric charge $2e$ in the above formula, whereas quantum vortices exist also in neutral quantum condensates where their currents $\vec{j}_{\text{vortex}} = n_s\vec{v}_s$ do not produce any magnetism. Thus, the presence of the singular line were the phase diverges is a more general property of the vortex than the magnetic flux.

The important thing is that 2π-phase singularities could be of both signs, that define vortices and antivortices, Fig. 8(a). Adding a vortex (antivortex) to any superconductor modifies the winding number by $+1$ (-1). This is only possible by breaking the phase coherence at the sample edge. That is why individual vortices (antivortices) cannot nucleate in the bulk. However, adding a vortex-antivortex pair directly inside a superconductor is topologically allowed as it does not change the total winding number. In nonmagnetic superconductors, such vortex-antivortex pairs are energetically unfavorable and do not appear (except at Berezinskii-Kosterlitz-Thouless-type transitions where they are theoretically predicted but not directly observed yet).

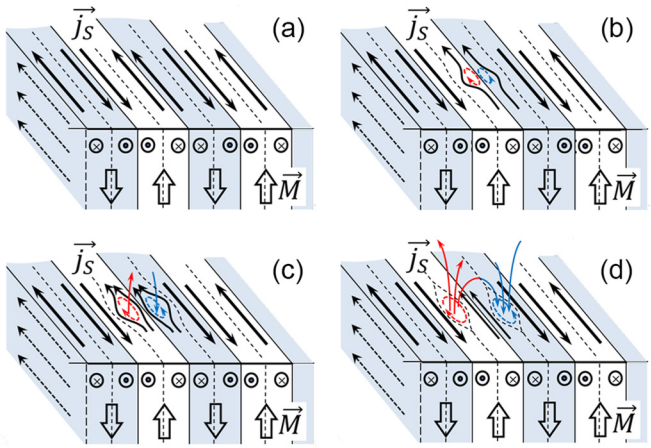

FIG. 9. Suggested vortex-antivortex pair nucleation in ferromagnetic superconductors ($T_c > T_{FM}$) and its detection by MFM. (a) and (b) the V-A pairs nucleate at the domain walls where the Meissner currents are strongest; (c) once the V-A pair emerges at surface vortices and antivortices split and become detectable by MFM; (d) the equilibrium vortex-antivortex pair position is situated close to centers of ferromagnetic domains. Note that in superconducting ferromagnets ($T_c < T_{FM}$) vortices and antivortices nucleate at T_c directly inside the respective FM domains.

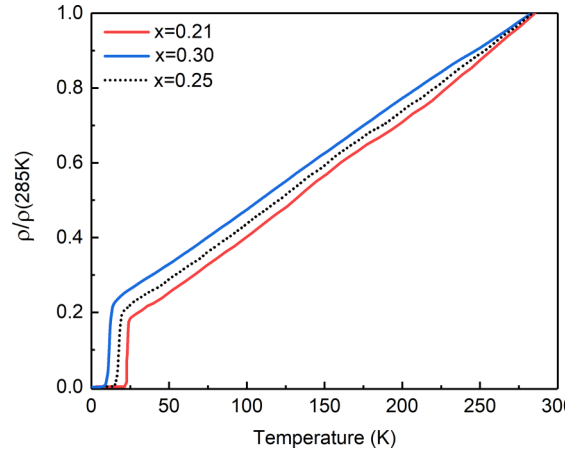

FIG. 10. Temperature dependence of the electric resistance of different P-doped $EuFe_2(As_{1-x}P_x)_2$ samples. See the text.

APPENDIX C: VORTEX-ANTIVORTEX PAIR NUCLEATION AND DETECTION

The MFM results of Ref. [8] witnessed for a local vortex-antivortex pair generation in Eu122 samples [see Fig. 3 therein; also displayed in the Supplemental Material [22] in Sec. A. Ferromagnetic superconductors, SFigs. 1(f)–1(q)] [22]. Although, MFM certainly misses the early stages of nucleation of V-A pairs as it detects vortices and antivortices only when they emerge at the surface and produce a detectable magnetic signal outside the sample [Figs. 9(c) and 9(d)]. So, where does the nucleation occur: At the surface or in the bulk? What are the shape and the spatial extend of this double phase singularity? Logically, it could be in a form of a tiny bundle of a size $\sim\xi$ as Fig. 8(b) suggests, or a doublet of phase singularity lines crossing the sample as in Fig. 8(c); other geometries cannot be excluded. Whereas the spatial evolution of the magnetic induction in our samples (presented in Fig. 3 of the main paper) seems to privilege the hypothesis of V-A nucleation by bundles (due to magnetic line reconnections), up to now neither theory nor experiments addressed this fundamental question.

APPENDIX D: ELECTRON TRANSPORT PROPERTIES

The temperature dependence of the electric resistance of the samples measured by the four-terminal method is presented in Fig. 10. The samples with $0.2 < x < 0.3$ showed similar quasilinear $R(T)$ dependence and superconductivity below 12–28 K, depending on P content. Note that because of a very small size of the $x = 0.25$ sample, its $R(T)$ dependence was not measured directly. The dashed line shows the expected behavior interpolated from the experimentally measured $R(T)$ in the $x = 0.21$ and $x = 0.3$samples. The superconducting critical temperature of the $x = 0.25$ sample was determined precisely from $M(T)$ experiments.

APPENDIX E: FINE STRUCTURE OF VORTEX DOMAINS IN THE $x = 0.25$ SAMPLE

The one-dimensional motion of vortices in the $x = 0.25$ sample results in several spectacular effects that need further theoretical input to be understood. First, the density of the vortex (antivortex) lattice in each domain (antidomain) is modulated along the domain walls as shown in Supplemental figures SFigs. 3(i)–3(k) [22] and visible in Fig. 11(a). As the temperature is lowered, both the modulation period and the modulation amplitude slightly increase. Second, the phases of modulations in neighboring vortex- and antivortex-containing domains coincide: Denser areas of vortex and antivortex lattices are located close to each other, reflecting their mutual attraction. Third, at low temperatures, a dimerization effect is observed: Modulated vortex lattice chains of opposite polarities get closer 2×2, Figs. 11(a)–(d). This points towards the existence of several instabilities in the phase diagram. Other effects are revealed in MFM maps; they are displayed and discussed in the Supplemental Material in Sect. B, the superconducting ferromagnet [22].

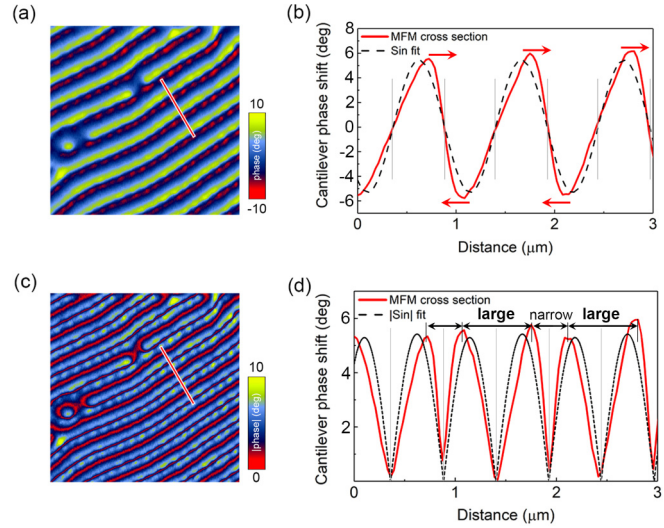

FIG. 11. "Dimerization" across domain walls of vortex-antivortex lattice modulations observed at low temperature (the $x = 0.25$ sample). (a) MFM map $8.8 \times 8.8\ \mu m^2$ acquired at 4.622 K. (b) Red curve: MFM phase shift profile over the path presented in (a). The profile is distorted as compared to symmetric sin fit (dashed line). Vertical lines denote the domain walls; red arrows show the distortion directions. (c) Map of the absolute value of phase of the map in (a). (d) Corresponding profile (red curve) and $|\sin|$ fit (dashed line). The dimerization results in shorter distances between the maxima of vortex-antivortex lattice density at each second domain wall.

[1] L. N. Bulaevskii, A. I. Buzdin, M. L. Kulic, and S. V. Panjukov, Adv. Phys. **34**, 175-261 (1985).

[2] Z. Ren, Q. Tao, S. Jiang, C. Feng, C. Wang, J. Dai, G. Cao, and Z. Xu, Phys. Rev. Lett. **102**, 137002 (2009).

[3] G. H. Cao, S. Xu, Z. Ren, S. Jiang, C. Feng, and Z. A. Xu, J. Phys.: Condens. Matter **23**, 464204 (2011).

[4] I. Nowik, I. Felner, Z. Ren, G. H. Cao, and Z. A. Xu, J. Phys.: Condens. Matter **23**, 065701 (2011).

[5] S. Zapf, D. Wu, L. Bogani, H. S. Jeevan, P. Gegenwart, and M. Dressel, Phys. Rev. B **84**, 140503(R) (2011).

[6] S. Zapf, H. S. Jeevan, T. Ivek, F. Pfister, F. Klingert, S. Jiang, D. Wu, P. Gegenwart, R. K. Kremer, and M. Dressel, Phys. Rev. Lett. **110**, 237002 (2013).

[7] S. Nandi, W. T. Jin, Y. Xiao, Y. Su, S. Price, D. K. Shukla, J. Strempfer, H. S. Jeevan, P. Gegenwart, and T. Bruckel, Phys. Rev. B **89**, 014512 (2014).

[8] V. S. Stolyarov, I. S. Veshchunov, S. Y. Grebenchuk, D. S. Baranov, I. A. Golovchanskiy, A. G. Shishkin, N. Zhou, Z. Shi, X. F. Xu, S. Pyon, Y. Sun, W. Jiao, G. H. Cao, L. Y. Vinnikov, A. A. Golubov, T. Tamegai, A. I. Buzdin, and D. Roditchev, Sci. Adv. **4**, eaat1061 (2018).

[9] L. Y. Vinnikov, I. S. Veshchunov, M. S. Sidel'nikov, V. S. Stolyarov, S. V. Egorov, O. V. Skryabina, W. Jiao, G. Cao, and T. Tamegai, JETP Lett. **109**, 521 (2019).
[10] G. Ghigo, D. Torsello, L. Gozzelino, T. Tamegai, I. S. Veshchunov, S. Pyon, W. Jiao, G. H. Cao, S. Y. Grebenchuk, I. A. Golovchanskiy, V. S. Stolyarov, and D. Roditchev, Phys. Rev. Research **1**, 033110 (2019).
[11] D. Aoki and J. Flouquet, J. Phys. Soc. Jpn. **81**, 011003 (2011).
[12] C. Paulsen, D. J. Hykel, K. Hasselbach, and D. Aoki, Phys. Rev. Lett. **109**, 237001 (2012).
[13] D. C. Johnston, Adv. Phys. **59**, 803 (2010).
[14] A. Pogrebna, T. Mertelj, N. Vujicic, G. Cao, Z. A. Xu, and D. Mihailovic, Sci. Rep. **5**, 7754 (2015).
[15] Z. Devizorova, S. Mironov, and A. Buzdin, Phys. Rev. Lett. **122**, 117002 (2019).
[16] D. E. Moncton, D. B. McWhan, P. H. Schmidt, G. Shirane, W. Thomlinson, M. B. Maple, H. B. MacKay, L. D. Woolf, Z. Fisk, and D. C. Johnston, Phys. Rev. Lett. **45**, 2060 (1980).
[17] J. W. Lynn, G. Shirane, W. Thomlinson, and R. N. Shelton, Phys. Rev. Lett. **46**, 368 (1981).
[18] I. S. Veshchunov, L. Y. Vinnikov, V. S. Stolyarov, N. Zhou, Z. X. Shi, X. F. Xu, S. Y. Grebenchuk, D. S. Baranov, I. A. Golovchanskiy, S. Pyon, Y. Sun, W. Jiao, G. Cao, T. Tamegai, and A. A. Golubov, JETP Lett. **105**, 98 (2017).
[19] H. S. Jeevan, D. Kasinathan, H. Rosner, and P. Gegenwart, Phys. Rev. B **83**, 054511 (2011).
[20] M. Faure and A. I. Buzdin, Phys. Rev. Lett. **94**, 187202 (2005).
[21] D. Wu, G. Chanda, H. S. Jeevan, P. Gegenwart, and M. Dressel, Phys. Rev. B **83**, 100503(R) (2011).
[22] See Supplemental Material at http://link.aps.org/supplemental/10.1103/PhysRevB.102.144501 for the full set of MFM images and an additional description.
[23] V. H. Dao, S. Burdin, and A. Buzdin, Phys. Rev. B **84**, 134503 (2011).
[24] M. Iavarone, A. Scarfato, F. Bobba, M. Longobardi, G. Karapetrov, V. Novosad, V. Yefremenko, F. Giubileo, and A. M. Cucolo, Phys. Rev. B **84**, 024506 (2011).
[25] F. Bobba, C. DiGiorgio, A. Scarfato, M. Longobardi, M. Iavarone, S. A. Moore, G. Karapetrov, V. Novosad, V. Yefremenko, and A. M. Cucolo, Phys. Rev. B **89**, 214502 (2014).
[26] C. Kittel, *Introduction to Solid State Physics* (Wiley, New York, 1967).
[27] L. Landau and E. Lifshitz, *Electrodynamics of Continuous Media* (Pergamon, Oxford, 1960).
[28] A. Hubert and R. Schafer, *Magnetic Domains, The Analysis of Magnetic Microstructures* (Springer-Verlag, Berlin/Heidelberg, 1998).
[29] A. Hubert and W. Rave, J. Magn. Magn. Mater. **196**, 325 (1999).
[30] M. M. Doria, A. R. de C. Romaguera, M. V. Milosevic, and F. M. Peeters, Europhys. Lett. **79**, 47006 (2007).
[31] F. Virot, L. Favre, R. Hayn, and M. D. Kuz'Min, J. Phys. D: Appl. Phys. **45**, 405003 (2012).